Journal of Biomechanics 44 (2011) 345–351

Contents lists available at ScienceDirect

Journal of Biomechanics

journal homepage: www.elsevier.com/locate/jbiomech
www.JBiomech.com

Characterization of structure and properties of bone by spectral measure method

Elena Cherkaev [a,*], Carlos Bonifasi-Lista [b]

[a] University of Utah, Department of Mathematics, 155 South 1400 East, JWB 233, Salt Lake City, UT 84112-0090, United States
[b] Universidad de Castilla-La Mancha, Departamento de Matematicas, E.T.S. Ingenieros Industriales, Ciudad Real, Spain

ARTICLE INFO

Article history:
Accepted 21 October 2010

Keywords:
Viscoelastic composite
Stieltjes representation
Spectral function
Inverse homogenization
Bone volume

ABSTRACT

Novel mathematical method called spectral measure method (SMM) is developed for characterization of bone structure and indirect estimation of bone properties. The spectral measure method is based on an inverse homogenization technique which allows to derive information about the structure of composite material from measured effective electric or viscoelastic properties. The mechanical properties and ability to withstand fracture depend on the structural organization of bone as a hierarchical composite. Information about the bone structural parameters is contained in the spectral measure in the Stieltjes integral representation of the effective properties. The method is based on constructing the spectral measure either by calculating it directly from micro-CT images or using measurements of electric or viscoelastic properties over a frequency range. In the present paper, we generalize the Stieltjes representation to the viscoelastic case and show how bone microstructure, in particular, bone volume or porosity, can be characterized by the spectral function calculated using measurements of complex permittivity or viscoelastic modulus. For validation purposes, we numerically simulated measured data using micro-CT images of cancellous bone. Recovered values of bone porosity are in excellent agreement with true porosity estimated from the micro-CT images. We also discuss another application of this method, which allows to estimate properties difficult to measure directly. The spectral measure method based on the derived Stieltjes representation for viscoelastic composites, has a potential for non-invasive characterization of bone structure using electric or mechanical measurements. The method is applicable to sea ice, porous rock, and other composite materials.

1. Introduction

Bone is a hierarchical composite whose ability to withstand fracture depends on the bone structural organization. At the microscale, cancellous bone is a heterogeneous composite formed of trabeculae with bone marrow filling its porous spaces (see Fig. 1). The macroscale mechanical properties such as bone stiffness and strength depend on bone microstructure, density, and stiffness of the bone tissue (Hollister et al., 1991; Crolet et al., 1993; Aoubiza et al., 1996; Lakes, 2001; Cowin, 2001; Hellmich et al., 2004). To analyze the dependence of the bone properties on its structure, trabecular architectures were idealized as open and close cell high porosity models (Gibson, 1985; Keaveny, 1997; Kabel et al., 1999b). Non-destructive imaging methods such as X-ray and micro-CT, have been developed to predict the mechanical properties of the bone from its structure by correlating measured by X-ray or CT structural parameters with results of mechanical tests or numerical simulations (Kabel et al., 1999a). Bone morphology was related with ultrasound propagation, methods aimed at numerical recovery of bone density and structural parameters from ultrasonic data have been developed (Chaffai et al., 2002; Padilla and Laugier, 2005; Padilla et al., 2008; Fang et al., 2007; Buchanan et al., 2003, 2004; Gilbert et al., 2009).

Mechanical properties of bone are linked with bone volume, fabric tensor, and anisotropy (Cowin, 1985; Hodgskinson and Currey, 1990; Zysset et al., 1998; Goulet et al., 1994; Van Rietbergen et al., 1998; Borah et al., 2000). Relationships between the elasticity tensor, structural density, and the invariants of the fabric tensor were developed in Cowin (1985), Turner et al. (1990) and Kabel et al. (1999a). Statistical correlations of structural and elastic parameters give significant correlation coefficients for particular bone samples; however, in general, they could be not applicable to another bone sample (Van Rietbergen et al., 1998; Van Rietbergen and Huiskies, 2001). Though the trabecular morphology determines the elastic properties of cancellous bone, not many analytical models are available to relate the properties and morphology (Kabel et al., 1999a).

Spectral measure method of characterization of bone structure is a method that provides relations between structural parameters and electric and viscoelastic properties. It is based on results of

* Corresponding author. Tel.: +1 801 581 7315; fax: +1 801 581 4148.
E-mail address: elena@math.utah.edu (E. Cherkaev).
URL: http://www.math.utah.edu/~elena/ (E. Cherkaev).

0021-9290/$ - see front matter © 2010 Elsevier Ltd. All rights reserved.
doi:10.1016/j.jbiomech.2010.10.031

Fig. 1. At the microscale, cancellous bone is a heterogeneous composite material formed of trabeculae and bone marrow. Photograph of trabecular bone is courtesy of Scott C. Miller.

forward and inverse homogenization for materials with microstructure. This method is not site specific, it relies neither on correlation analysis nor on assumptions about a particular morphology of bone. Based on analytical relations and characterization of resonances of the bone structure, spectral measure method provides a basis for relating microstructural parameters to effective electric, elastic, and viscoelastic behavior of bone as well as for modeling and predicting bone structure from electrical, mechanical, and potentially, ultrasound data.

Mechanical behavior of a composite material depends on properties of the components as well as on the microarchitecture. Various approaches to calculation of effective properties from known microstructural information, have been developed using homogenization theory (Sanchez-Palencia, 1980; Hollister et al., 1994; Bergman, 1993; Zoui, 2002; Milton, 2002). One of the methods developed for bounding the effective complex permittivity of a composite formed by two materials with given complex permittivity, used the analytic Stieltjes representation of the effective property (Bergman, 1978, 1980; Milton, 1980; Golden and Papanicolaou, 1983). The Stieljtes representation analytically relates the effective properties to microstructural information through the spectrum of a corresponding linear operator. Specifically, the moments of the spectral measure in this representation are linked to the n-point correlation functions of the microstructure. Another important feature of the Stieltjes representation of the effective properties is that it factors out the dependence on the constituents in the composite from the dependence on the microgeometry. The information about the microstructure is contained in the spectral measure in the Stieltjes representation of the effective properties. This feature of the Stieltjes representation allows us to recover microstructural parameters from effective properties using inverse homogenization. The inverse homogenization is based on the recovery of the spectral measure which contains information about the microgeometry (Cherkaev, 2001). Once the spectral measure is known, it can be used to characterize the bone morphology. The spectral measure can be constructed directly from the images obtained from regular CT or micro-CT, or it can be recovered from non-invasive electric or viscoelastic measurements over a range of frequencies.

The problem of extraction of structural information from measured transport properties of composite materials was introduced in McPhedran et al. (1982) for estimating volume fractions of constituents in the composite. In Cherkaev (2001), identification of structural information from measured effective property was formulated as an inverse problem for the spectral measure in the Stieltjes analytic representation. It was shown that the spectral measure can be uniquely recovered from the measurements of the effective property over a range of frequencies (Cherkaev, 2001). Uniqueness of reconstruction of the spectral measure gives the basis for the theory of inverse homogenization and the spectral measure method (SMM). The term SMM was coined in Bonifasi-Lista and Cherkaev (2009), where the method was used to estimate bone porosity from data of complex conductivity of bone samples numerically simulated using micro-CT images.

The analytic Stieljtes representation was extended to the effective elastic properties of a composite material in Kantor and Bergman (1982, 1984), Bergman (1985), Dell'Antonio et al. (1986), Bruno and Leo (1993), Milton (2002) and Ou and Cherkaev (2006). Stieltjes representation for the effective viscoelastic shear modulus obtained from torsion of a viscoelastic cylinder whose microstructure does not depend on the axial direction, was derived in Tokarzewski et al. (2001), Bonifasi-Lista and Cherkaev (2006a, b, 2008), assuming St.Venant principle and using mathematical equivalency between conductivity problem and elastic torsion of such cylinder. In Tokarzewski et al. (2001), this representation was used to bound the effective shear modulus of cancellous bone filled with bone marrow. Based on this representation, the inverse homogenization approach was applied in Bonifasi-Lista and Cherkaev (2006a, b, 2008), and Bonifasi-Lista et al. (2009) to successfully recover porosity of cancellous and compact bone from simulated measurements of the viscoelastic shear modulus for the simplified model of bone viewed as a cylinder, filled with viscoelastic composite of trabecular tissue and bone marrow, realistic data were simulated using micro-CT images of cancellous bone.

2. Mathematical methods

2.1. Spectral measure method

We consider bone as a two component composite formed by trabecular tissues and bone marrow and introduce a characteristic function χ of the subdomains occupied by one of the materials. In bioelectrical applications, low frequency electric fields are used in practice, the appropriate parameter characterizing properties of the medium, is complex conductivity σ. The complex conductivity σ of the medium is modeled by a function $\sigma(\mathbf{x}) = \sigma_1\chi(\mathbf{x}) + \sigma_2(1-\chi(\mathbf{x}))$, where $\sigma_i, i = 1,2$, is complex conductivity of the i-th material, bone marrow or trabecular tissue, and the characteristic function $\chi = \chi(\mathbf{x})$ takes values 1 if $\mathbf{x}$ is in the region of first material, bone marrow, and zero if $\mathbf{x}$ is in the region occupied by the second material. The effective tensor $\boldsymbol{\sigma}^*$ is a coefficient of proportionality between the averaged electric and displacement fields: $\langle J \rangle = \sigma^* \langle E \rangle$, and the electric field is governed by equation: $\nabla \cdot (\sigma_1\chi(\mathbf{x}) + \sigma_2(1-\chi(\mathbf{x})))E = 0$. Introducing $s = 1/(1-\sigma_1/\sigma_2)$, the derivation of the Stieltjes representation uses a spectral decomposition of an operator $\Gamma\chi = \nabla(-\Delta)^{-1}(\nabla\cdot)\chi$, and results in the integral representation for a function $F(s) = 1-\sigma^*/\sigma_2$ as an analytic function off [0, 1)-interval in the complex s-plane:

$$F(s) = \int_0^1 \frac{d\eta(z)}{s-z} \tag{1}$$

Here the function η is the spectral measure of the self-adjoint operator $\Gamma\chi$, which contains information about the structural parameters. The spectral function η can be uniquely reconstructed if measurements of the effective properties of the composite are known along some arc in the complex s-plane (Cherkaev, 2001). Such data can be obtained from effective measurements in an interval of frequency provided the properties of the constituents are dependent on frequency. The spectral moments η_n of the spectral measure η,

$$\eta_n = \int_0^1 z^n \, d\eta(z), \quad \eta_0 = \int_0^1 d\eta(t) = p_1 \tag{2}$$

can be used to characterize the microgeometry of bone. In particular, the zero moment η_0 of the function η gives us the volume fraction p_1 of the first component, bone marrow or trabecular tissue, depending on how the problem is formulated.

A representation similar to (1), is valid for torsion of a viscoelastic cylinder in which the microstructure does not depend on the axial direction. If the effective viscoelastic shear modulus of such composite is given by a complex number μ^*, and $\mu_i, i=1,2$, are the complex shear moduli of the constituents, the Stieltjes representation (1) holds for a function $F_\mu(s)=1-\mu^*/\mu_2$ with $s=1/(1-\mu_1/\mu_2)$.

The spectral function η in the representation (1) relates various properties of the composite. If the function η is known from the electric measurements, the effective viscoelastic modulus of bone can be easily estimated by calculating the following integral:

$$\mu^*=\mu_2-\mu_2F_\mu(s)=\mu_2-\mu_2\int_0^1\frac{d\eta(z)}{s-z} \tag{3}$$

with $s=1/(1-\mu_1/\mu_2)$. An example of such relation or coupling between complex permittivity and thermal conductivity was considered in Cherkaev (2003) and Cherkaev and Zhang (2003), where thermal conductivity of sandstone was estimated using measurements of its effective permittivity. This spectral coupling might provide a way to indirectly calculate bone properties which are difficult to access directly, such as thermal conductivity, diffusion, or bone permeability.

2.2. Stieltjes analytical representation for viscoelastic properties

Here we generalize the Stieltjes representation for effective viscoelastic modulus to the case of general loading. In particular, this representation works for uniaxial loading which is an important case in various experimental setups. We assume that (i) the constituents are isotropic materials with the same elastic bulk modulus κ, (ii) one of the materials (bone marrow) has viscoelastic shear modulus μ_1, (iii) the shear modulus μ_2 of the second material (trabecular tissues) is elastic. We use here the Einstein summation convention of summing on repeated indices.

Let Ω be a domain filled with a heterogeneous material composed of two phases, viscoelastic material C^1 in a subdomain Ω_1 and elastic phase C^2 in the region Ω_2. Consider a boundary value problem for vector of displacement u in a domain Ω with boundary $\partial\Omega$:

$$\sigma_{ij,j}=0 \quad \text{in } \Omega \tag{4}$$

$$\sigma_{ij}=C_{ijkl}\varepsilon_{kl} \quad \text{in } \Omega \tag{5}$$

$$u_i=\varepsilon^0_{ij}x_j \quad \text{on } \partial\Omega \tag{6}$$

Here ε and σ are tensors of strain and stress, respectively, strain ε is a symmetrized gradient ∇^s of displacement, $\varepsilon=\nabla^s u=(\nabla u+\nabla u^T)/2$, and ε^0 is a constant strain tensor. The fourth order tensor C is the stiffness tensor which depends on the properties of the phases and the characteristic function $\chi=\chi(\mathbf{x})$ of domain Ω_1 occupied by bone marrow tissue, the function $\chi(\mathbf{x})$ takes values 1 if $\mathbf{x}\in\Omega_1$ and zero if $\mathbf{x}\in\Omega_2$, where Ω_2 is the region occupied by the trabecular tissue. Using this function χ, we represent the tensor C as $C(\mathbf{x})=\chi(\mathbf{x})C^1+(1-\chi(\mathbf{x}))C^2$. Without loss of generality, we assume that the domain Ω has unit volume, $|\Omega|=1$, and introduce an operation of averaging $\langle f\rangle$ of a function f over the domain Ω, $\langle f\rangle=\int_\Omega f(x)\,dx$. We notice that solution of the problems (4)–(6) satisfies $\langle\varepsilon\rangle=\varepsilon^0$.

The effective viscoelastic tensor C^* is introduced as a coefficient of proportionality between the average strain and stress. Using Eq. (5), the average stress $\langle\sigma\rangle$ can be written as

$$\langle\sigma_{ij}\rangle=\int_\Omega\sigma_{ij}(\mathbf{x})\,dV=C^*_{ijkl}\varepsilon^0_{kl} \tag{7}$$

here,

$$C^*_{ijkl}=\int_\Omega C_{ijmn}(\mathbf{x})\varepsilon^{(kl)}_{mn}(\mathbf{x})\,dV \tag{8}$$

and

$$C^*_{ijkl}\varepsilon^0_{kl}=\int_\Omega C_{ijmn}(\mathbf{x})\varepsilon^{(kl)}_{mn}(\mathbf{x})\varepsilon^0_{kl}\,dV=\int_\Omega C_{ijmn}(\mathbf{x})\varepsilon_{mn}(\mathbf{x})\,dV \tag{9}$$

Using contraction notation, this can be written as

$$C^*:\varepsilon^0=C^*_{ijkl}\varepsilon^0_{kl}=\int_\Omega C_{ijmn}(\mathbf{x})\varepsilon_{mn}(\mathbf{x})\,dV=\int_\Omega C(\mathbf{x}):\varepsilon(\mathbf{x})\,dV \tag{10}$$

Isotropic elastic (or viscoelastic) tensor can be represented as

$$C_{ijkl}=\kappa\delta_{ij}\delta_{kl}+\mu(\delta_{ik}\delta_{jl}+\delta_{il}\delta_{jk}-\tfrac{2}{3}\delta_{ij}\delta_{kl}) \tag{11}$$

We introduce isotropic fourth order projection tensors Λ_h and Λ_s as

$$\{\Lambda_h\}_{ijkl}=\delta_{ij}\delta_{kl},\quad \{\Lambda_s\}_{ijkl}=\delta_{ik}\delta_{jl}+\delta_{il}\delta_{jk}-\frac{2}{3}\delta_{ij}\delta_{kl} \tag{12}$$

Here, δ_{ij} is the Kronecker delta. The tensors Λ_h and Λ_s are hydrostatic and deviatoric projections onto the orthogonal subspaces of the second order tensors comprised of tensors proportional to the identity and trace-free tensors. Using these projections, the isotropic properties C^i of materials in the domain Ω_i can be written as

$$C^i=\kappa\Lambda_h+\mu_i\Lambda_s,\quad i=1,2 \tag{13}$$

Now we rewrite problem (4) in the following form:

$$\nabla\cdot(\chi(\mathbf{x})C^1+(1-\chi(\mathbf{x}))C^2):\varepsilon=0 \tag{14}$$

Using (13) we have

$$\nabla\cdot(\kappa\Lambda_h+(\mu_1\chi(\mathbf{x})+(1-\chi(\mathbf{x}))\mu_2)\Lambda_s):\varepsilon=0 \tag{15}$$

Eq. (15) can be written in terms of a complex parameter s, $s=\mu_2/(\mu_2-\mu_1)$, as

$$\nabla\cdot\left(\frac{\kappa}{\mu_2}\Lambda_h+\left(1-\frac{1}{s}\chi\right)\Lambda_s\right):\varepsilon=0 \tag{16}$$

By writing ε as $\varepsilon=\varepsilon^0+\nabla^s\phi$, where ϕ is vector perturbation, and using $\kappa_2=\kappa/\mu_2$, we obtain

$$\nabla\cdot(\kappa_2\Lambda_h+1\Lambda_s):(\varepsilon^0+\nabla^s\phi)=\frac{1}{s}\nabla\cdot\chi\Lambda_s:(\varepsilon^0+\nabla^s\phi) \tag{17}$$

The operator in the left-hand side is elastic operator with constant coefficients, denoting it as $L(\kappa_2,1)\phi=\nabla\cdot(\kappa_2\Lambda_h+1\Lambda_s):\nabla^s\phi$, we can rewrite the last problem in the following form:

$$L(\kappa_2,1)\phi=\frac{1}{s}\nabla\cdot\chi\Lambda_s:(\varepsilon^0+\nabla^s\phi) \tag{18}$$

Let $G=(-L(\kappa_2,1))^{-1}$ be the tensor Green's operator for the isotropic elastic problem with constant bulk modulus κ_2 and constant unit shear modulus. Applying G to both sides of the previous equation, then taking gradient and adding ε^0, we obtain

$$(\nabla^s\phi+\varepsilon^0)-\frac{1}{s}\nabla^sG\nabla\cdot\chi\Lambda_s:(\varepsilon^0+\nabla^s\phi)=\varepsilon^0 \tag{19}$$

Introducing operator $\mathcal{G}$ as $\mathcal{G}=\nabla^sG(\nabla\cdot)$, we express the strain ε as a function of $\mathcal{G}\chi\Lambda_s$

$$\varepsilon-\frac{1}{s}\mathcal{G}\chi\Lambda_s:\varepsilon=\varepsilon^0 \tag{20}$$

We will take projection on deviatoric subspace

$$\Lambda_s:\varepsilon-\frac{1}{s}\Lambda_s:\mathcal{G}\chi\Lambda_s:\varepsilon=\Lambda_s:\varepsilon^0 \tag{21}$$

Let ε_s be deviatoric projection of the strain ε, $\varepsilon_s = \Lambda_s : \varepsilon$. Using idempotence of projection operator, $\Lambda_s^2 = \Lambda_s$, we obtain

$$\left(I - \frac{1}{s}\Lambda_s : \mathcal{G}\chi\Lambda_s\right) : \varepsilon_s = \varepsilon_s^0 \tag{22}$$

so that $\varepsilon_s = s(sI - \Lambda_s : \mathcal{G}\chi\Lambda_s)^{-1} : \varepsilon_s^0$.

We notice here that introduced in this way operator $\mathcal{G} = \nabla^s G(\nabla\cdot)$ with $G = (-L(\kappa_2,1))^{-1}$, is the analogue for elasticity of the operator $\Gamma = \nabla(-\Delta)^{-1}(\nabla\cdot)$ used in the problem for effective complex conductivity.

The stiffness tensor in $L(\kappa_2,1)$ is real symmetric tensor. We can check that $\Lambda_s : \mathcal{G}\chi\Lambda_s$ is a self-adjoint operator with respect to inner product $\langle f,g \rangle = \langle \chi \bar{f}_{ij} g_{ij} \rangle$ where f, g are second order symmetric strain tensors. We use $\bar{f}$ to denote the complex conjugate of f, and $\langle . \rangle$ is the averaging operator.

Then we can use spectral representation and write ε_s as

$$\varepsilon_s = \int_0^1 \frac{s(dQ(z)\Lambda_s\varepsilon^0)}{s-z} \tag{23}$$

where Q is the projection valued measure of the operator $\Lambda_s\mathcal{G}\chi\Lambda_s$. Now exploiting this integral representation for ε_s and using $\varepsilon_s^0 = \Lambda_s : \varepsilon^0$, we derive spectral representation for function $F(s)$ which we define as

$$F(s) = \frac{\varepsilon^0 : C^2 : \varepsilon^0 - \varepsilon^0 : C^* : \varepsilon^0}{\varepsilon_s^0 : C^2 : \varepsilon_s^0} = \frac{\varepsilon_{ij}^0 C_{ijkl}^2 \varepsilon_{kl}^0 - \varepsilon_{ij}^0 C_{ijkl}^* \varepsilon_{kl}^0}{\mu_2 \|\varepsilon_s^0\|^2} \tag{24}$$

since $\varepsilon_s^0 : C^2 : \varepsilon_s^0 = \mu_2 \varepsilon_s^0 : \varepsilon_s^0 = \mu_2 \|\varepsilon_s^0\|^2$.

A direct calculation using (24) gives

$$F(s)\mu_2\|\varepsilon_s^0\|^2 = \varepsilon^0 : C^2 : \varepsilon^0 - \varepsilon^0 : \int_\Omega C(x) : \varepsilon(x) = \tag{25}$$

$$\varepsilon^0 : C^2 : \varepsilon^0 - \varepsilon^0 : C^2 : \varepsilon^0 + \varepsilon^0 : \mu_2 \int_\Omega \frac{1}{s}\chi\Lambda_s : \varepsilon(x) = \tag{26}$$

$$\varepsilon^0 : \int_\Omega \int_0^1 \frac{1}{s}\chi\Lambda_s \frac{s\mu_2(dQ(z)\Lambda_s : \varepsilon^0)}{s-z} = \int_0^1 \frac{\mu_2 \langle dQ(z)\varepsilon_s^0, \varepsilon_s^0 \rangle}{s-z} \tag{27}$$

where we used definition of the inner product in the last step. Let e_s be a unit strain tensor:

$$e_s = \frac{\Lambda_s : \varepsilon^0}{\|\Lambda_s : \varepsilon^0\|} = \frac{\varepsilon_s^0}{\|\varepsilon_s^0\|} \tag{28}$$

then we can rewrite the integral representation for $F(s)$ as

$$F(s) = (\mu_2\|\varepsilon_s^0\|^2)^{-1} \int_0^1 \frac{\mu_2 \langle dQ(z)\varepsilon_s^0, \varepsilon_s^0 \rangle}{s-z} \tag{29}$$

$$= \|\varepsilon_s^0\|^{-2} \int_0^1 \frac{\langle dQ(z)e_s, e_s \rangle \|\varepsilon_s^0\|^2}{s-z} = \int_0^1 \frac{\langle dQ(z)e_s, e_s \rangle}{s-z} \tag{30}$$

By introducing the spectral measure $d\eta(z) = \langle dQ(z)e_s, e_s \rangle$, we obtain the representation

$$F(s) = \frac{\varepsilon^0 : C^2 : \varepsilon^0 - \varepsilon^0 : C^* : \varepsilon^0}{\varepsilon_s^0 : C^2 : \varepsilon_s^0} = \int_0^1 \frac{d\eta(z)}{s-z} \tag{31}$$

The derived representation allows us to extend the theory to mechanical and ultrasonic applications.

2.3. *Inverse problem for the spectral measure*

Information about bone morphology is contained in the spectral measure of the Stieltjes representation and in the spectral moments. Evaluation of first several moments of the spectral function was discussed in McPhedran et al. (1982), McPhedran and Milton (1990), Engstrom (2006), and Cherkaev and Ou (2008), analytic inverse bounds on the volume fraction of one material in the composite were derived in Cherkaeva and Tripp (1996), Tripp et al. (1998), and Cherkaeva and Golden (1998), the spectral function was reconstructed from effective permittivity in particular applications (Day and Thorpe, 1999; Day et al., 2000; Cherkaev and Zhang, 2003; Zhang and Cherkaev, 2008). The problem of reconstruction of the spectral measure is ill-posed, which means instability of the solution to small errors in the measurements, therefore a regularized algorithm is needed to recover a stable numerical solution (Cherkaev, 2001, 2003; Zhang and Cherkaev, 2009).

Computation of the spectral function η is mathematically analogous to the analytic continuation and inverse potential problem. Indeed, the reconstruction of the spectral measure η can be reduced to an inverse potential problem by representing the function $F(s)$ using logarithmic potential of the measure η (Cherkaev, 2001)

$$F(s) = \frac{\partial}{\partial s}\int_0^1 \ln|s-z|\, d\eta(z), \quad \partial/\partial s = (\partial/\partial x - i\partial/\partial y) \tag{32}$$

To construct the solution we formulate the minimization problem: $\|A\eta - F\| \to \min$ where A is the integral operator in (32). Ill-posedness of the problem manifests itself in the absence of continuous dependence of the solution on the data: the operator A^{-1} is unbounded, this leads to large variations in the solution even for very small variations in the data, numerical algorithms become unstable, the problem requires regularization. Regularization algorithm is based on constrained minimization. It introduces a stabilization functional which constrains the set of minimizers. As a result, the solution depends continuously on the input data, the numerical algorithm is stable. Introducing $s = x + iy$ and separating real and imaginary parts of function $F(s)$, we obtain

$$\mathrm{Re}(F(s)) = \int_0^1 \frac{(x-z)\, d\eta(z)}{(x-z)^2 + y^2}, \quad \mathrm{Im}(F(s)) = -\int_0^1 \frac{y\, d\eta(z)}{(x-z)^2 + y^2} \tag{33}$$

We reformulate the problem as an unconstrained minimization using a Lagrange multiplier. In case of a quadratic stabilization functional, the minimization problem takes the following form equivalent to Tikhonov regularization with regularization parameter α : $\min_{g \in R^n}\{\|Kg - f\|_2^2 + \alpha\|g\|_2^2\}$. Here K is discretized integral operator corresponding to real or imaginary part of $F(s)$ in integral representation (33). Function f is either real or imaginary part of $F(s)$ obtained experimentally, and g is the discretization of $d\eta(z) = g(z)dz$. One of the ways to find the minimizer is to solve the Euler equation, $g_\alpha = (K^*K + \alpha I)^{-1}K^*f$. An alternative regularization algorithm uses nonnegativity constraint for function g. Indeed, the spectral measure in (1) is a nondecreasing function, hence g is a nonnegative function. Both these methods give similar results in the numerical experiments we describe in the next section.

3. Results

For validation of the method, we simulated data using micro-CT images of trabecular bone. The effective complex permittivity, effective complex shear modulus, and Young modulus of the 2D bone samples were calculated using finite element method. One of the micro-CT images is shown in Fig. 2. The effective shear and Young moduli were calculated assuming cylinder model with properties constant along the axial direction. For the electrical problem, we used available data on conductivity and permittivity of trabecular and marrow tissues (Gabriel et al., 1996a, b). We assumed that σ_1 was the complex conductivity of the bone tissues, and σ_2 was the complex conductivity of bone marrow.

In the first series of numerical experiments, simulated conductivity values were used as data for the spectral measure reconstruction algorithm. Fig. 3 presents spectral function for bone sample shown in the micro-CT image in Fig. 2. The spectral function was calculated from real and imaginary parts of $F(s)$

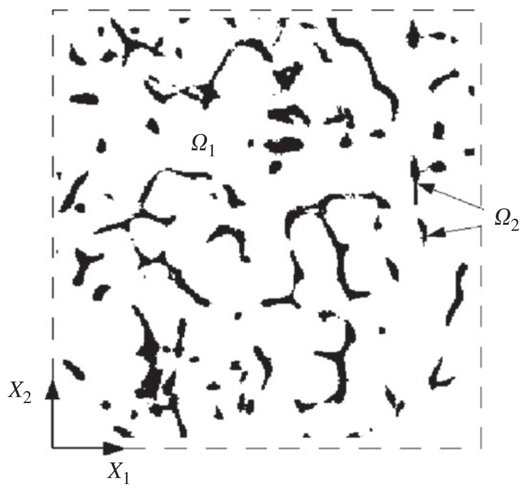

Fig. 2. One of the micro-CT images of a T12 vertebra used in the numerical simulations. The subdomain Ω_1 is filled with bone marrow, Ω_2 is filled with trabecular tissue. Micro-CT images are courtesy of Yener N. Yeni and his group.

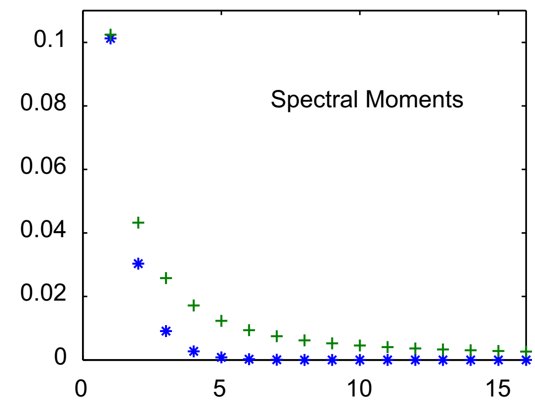

Fig. 4. Moments of the spectral function shown in Fig. 3. The bone structure moments are given by the pluses. For comparison, asterisks show moments of the spectral function of Maxwell–Garnett composite of the same porosity. Large difference between the sequences of the moments suggests that the spectral moments can be used to characterize the bone structure.

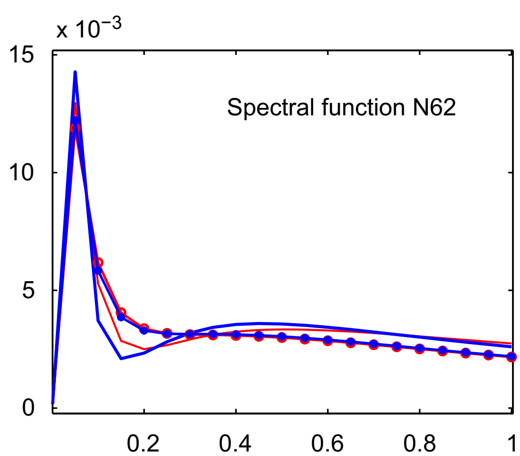

Fig. 3. Spectral function calculated from real and imaginary parts of $F(s)$ for the bone sample shown in the micro-CT image (see Fig. 2). Numerically simulated data for complex conductivity were used. Different curves correspond to the functions recovered using different techniques.

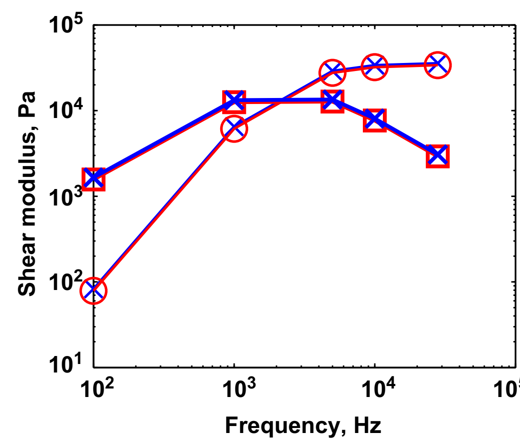

Fig. 5. Complex shear modulus of the bone sample shown in the micro-CT image (see Fig. 2) recovered from the real part of the complex conductivity of this sample. Crosses show recovered properties, circles/squares mark the true properties simulated directly from the micro-CT image. Real part is shown by circles, squares indicate imaginary part.

Table 1
Calculated estimates of bone volume V_{true} for several bone samples using electric data.

V_{true}	V_{RT}	V_{IT}	V_{RN}	V_{IN}	V_{av}
0.0740	0.0777	0.0753	0.0757	0.0759	0.0762
0.0743	0.0746	0.0713	0.0751	0.0729	0.0734
0.0755	0.0743	0.0763	0.0743	0.0763	0.0753
0.1012	0.1041	0.1009	0.1041	0.1010	0.1025

V_{RT} and V_{IT} columns show results of calculation using Tikhonov regularization, V_{RN} and V_{IN} stand for results with nonnegativity constraint, R or N in the heading indicates real or imaginary part of $F(s)$ used in calculation, V_{av} is the average bone volume.

using Tikhonov and nonnegativity regularization. We used recovered spectral function to estimate bone volume by calculating zeroth moment of the function η.

Results presented in Table 1, show that the bone volume is recovered very accurately with an error less than 0.1%. Table 1 shows the recovered volume fraction of trabeculae V for four different specimens of trabecular bone. True porosity of the samples was determined digitally from micro-CT scans.

The reconstructed spectral function can be characterized by its spectral moments. Fig. 4 shows moments of the spectral function presented in Fig. 3. The bone spectral moments are given by the pluses. For comparison, asterisks show moments of the spectral function of Maxwell–Garnett composite of the same porosity. Maxwell–Garnett composite is a composite with well-separated inclusions, its effective conductivity is given by an analytic formula. This composite has a very different structure. The corresponding sequences of the moments shown in Fig. 4 are quite different as well. Large difference between the sequences of the moments indicates that the spectral moments can be used to characterize the bone structure.

The next series of numerical experiments was performed to verify the spectral coupling by comparing complex shear modulus calculated using spectral function recovered from electric data, and viscoelastic shear modulus computed using FEM. To calculate viscoelastic properties of bone, we considered cancellous bone as a composite of trabecular tissue and bone marrow. We used the model of viscoelastic shear modulus for bone marrow developed in Bonifasi-Lista et al. (2009). Comparison of the shear values obtained with two different methods is presented in Fig. 5.

To study the integral representation derived in Section 2, we numerically simulated measurements of Young modulus for the

Table 2
Calculated estimates of bone porosity P_{true} for several bone samples using simulated measurements of Young modulus.

P_{true}	P_{RT}	P_{RN}	P_{av}
0.8987	0.8758	0.8900	0.8829
0.9245	0.9066	0.9227	0.9147
0.9257	0.9025	0.9184	0.9104
0.9338	0.9072	0.9233	0.9152

P_{RT} and P_{RN} columns show results of calculation using Tikhonov and nonnegative regularization, P_{av} is the calculated average porosity.

same 2D samples due to uniaxial loading. The Young modulus data were used to calculate the corresponding function $F(s)$ (31) and to recover elastic spectral function η in Eq. (31) by solving inverse problem for the real part of the integral equation. The zeroth moment of the function η gives us the porosity of bone. In Table 2, we show estimates P_{RT}, P_{RN}, and their average P_{av}, of bone porosity P_{true}, calculated from simulated measurements of Young modulus. The numerically predicted porosity values are in good agreement with the true values.

4. Discussion

Our viscoelastic representation derived in Section 2 uses an assumption of equality of the bulk moduli of the components. This assumption allows us to simplify the problem and make it amendable to mathematical analysis. We believe that the assumption of equal bulk moduli should not be too restrictive because the largest difference is in shear moduli of trabeculae and marrow. The ratio of the bulk modulus of solid bone matrix (14 GPa) and the bulk modulus of bone water or marrow (2.3 GPa) is around six. In comparison, the ratio of shear moduli is of order 10^8 (shear modulus of bone is 5 GPa, of marrow is around 200 Pa). The developed representation extends the theory to other applications such as creep experiments and ultrasonic testing.

In all calculations, we used data without noise, only computational noise was present. The method requires a priori knowledge of the properties of trabeculae tissue and marrow, which in practice could be known with some uncertainty, since these properties are subject-specific and depend on pathologic conditions. Extensive study of stability of the algorithm in Bonifasi-Lista and Cherkaev (2008) and Bonifasi-Lista et al. (2009), shows that the bone porosity is accurately recovered even in the presence of high level of uncertainty or errors in the data and estimates of the properties.

We notice that the electric and elastic spectral functions are different functions. However, they coincide in the case of torsion of a cylinder whose microstructure does not depend on the axial direction. Calculations of viscoelastic properties from electric spectral function, were performed with assumption that the microgeometry does not change along the third direction. This simplified bone model allows us to see new effects in modeling relations between bone's heterogeneous structure and effective electric and viscoelastic properties. Calculated from electric spectral function, the SMM prediction of the complex viscoelastic shear modulus and the FEM simulated modulus are in excellent agreement. The method of estimation of viscoelastic modulus from electric data might provide a non-invasive tool to assess fracture risk in bones. These numerical results demonstrate potential for use of the SMM for indirect evaluation of bone properties which are difficult to measure directly.

In the present paper, all calculations were done in 2D. In 3D case, we can use the same inversion method for the spectral measure, but to simulate the measurements we need to solve the 3D forward problem, which is computationally more intensive. In general case of 3D material, the viscoelastic spectral function is different from the electric spectral function. We expect that the electric and elastic spectral functions of bone should be similar because they correspond to the same trabecular structure, however, establishing relations between them is a future research topic. Another future direction of research is to relate the recovered spectral function and its moments to clinically relevant parameters of characterization of cancellous bone architecture such as trabeculae thickness, spacing, connectivity, surface density.

Conflict of interest statement

The authors declare that there is no conflict of interest associated with this work.

Acknowledgements

We would like to thank Yener N. Yeni and Janardhan Yerramshetty for providing micro-CT images of cancellous bone that we used in numerical simulations. We are also thankful to Maria-Grazia Ascenzi for helpful comments and Scott Miller for providing us with a photograph of cancellous bone. This research was partially supported by NSF Grant DMS/CMG-0934721.

References

Aoubiza, B., Crolet, J.M., Meunier, A., 1996. On the mechanical characterization of compact bone structure using the homogenization theory. Journal of Biomechanics 29, 1539–1547.
Bergman, D.J., 1978. The dielectric constant of a composite material—a problem in classical physics. Physics Reports C 43, 377–407.
Bergman, D.J., 1980. Exactly solvable microscopic geometries and rigorous bounds for the complex dielectric constant of a two-component composite material. Physical Review Letters 44, 1285.
Bergman, D.J., 1985. Bulk physical properties of composite media. In: Les méthodes de l'homogénéisation: théorie et applications en physique. Eyrolles, Paris, pp. 1–128.
Bergman, D.J., 1993. Hierarchies of Stieltjes functions and their applications to the calculation of bounds for the dielectric constant of a two-component composite medium. SIAM Journal on Applied Mathematics 53, 915–930.
Bonifasi-Lista, C., Cherkaev, E., 2006a. Identification of bone microstructure from effective complex modulus. In: Inan, E., Kiris, A. (Eds.), Vibration Problems ICOVP 2005, Springer Proceedings in Physics, vol. 111, pp. 91–96.
Bonifasi-Lista, C., Cherkaev, E., 2006b. Identification of bone microstructure from effective measurements. In: Proceedings of the Third European Conference on Computational Mechanics, Solids, Structures and Coupled Problems in Engineering, National Laboratory of Civil Engineering Portugal, Lisbon.
Bonifasi-Lista, C., Cherkaev, E., 2008. Analytical relations between effective material properties and microporosity: application to bone mechanics. International Journal of Engineering Science 46, 1239–1252.
Bonifasi-Lista, C., Cherkaev, E., 2009. Electrical impedance spectroscopy as a potential tool for recovering bone porosity. Physics in Medicine and Biology 54, 3063–3082.
Bonifasi-Lista, C., Cherkaev, E., Yeni, Y.N., 2009. Analytical approach to recovering bone porosity from effective complex shear modulus. Journal of Biomechanical Engineering 131, 121003-1–121003-8.
Borah, B., Dufresne, T.E., Cockman, M.D., Gross, G.J., Sod, E.W., Myers, W.R., 2000. Evaluation of changes in trabecular bone architecture and mechanical properties of minipig vertebrae by three-dimensional magnetic resonance microimaging and finite element modeling. Journal of Bone and Mineral Research 15, 1786–1797.
Bruno, O.P., Leo, P.H., 1993. On the stiffness of materials containing a disordered array of microscopic holes or hard inclusions. Archive for Rational Mechanics and Analysis 121, 303–338.
Buchanan, J.L., Gilbert, R.P., Wirgin, A., Xu, Y., 2003. Transient reflection and transmission of ultrasonic waves in cancellous bones. Applied Mathematics and Computation, 561–573.
Buchanan, J.L., Gilbert, R.P., Khashanah, K., 2004. Determination of the parameters of cancellous bone using low frequency acoustic measurements. Journal of Computational Acoustics 12 (2), 99–126.
Chaffai, S., Peyrin, F., Nuzzo, S., Porcher, R., Berger, G., Laugier, P., 2002. Ultrasonic characterization of human cancellous bone using transmission and backscatter measurements: relationships to density and microstructure. Bone 30 (1), 229–237.

Cherkaeva, E., Tripp, A.C., 1996. Bounds on porosity for dielectric logging. In: Proceedings of the Ninth Conference of the European Consortium for Mathematics in Industry, Technical University of Denmark, Denmark, Copenhagen.
Cherkaeva, E., Golden, K., 1998. Inverse bounds for microstructural parameters of a composite media derived from complex permittivity measurements. Waves in Random Media 8, 437–450.
Cherkaev, E., 2001. Inverse homogenization for evaluation of effective properties of a mixture. Inverse Problems 17, 1203–1218.
Cherkaev, E., 2003. Spectral coupling of effective properties of a random mixture. In: Movchan, A.B. (Ed.), IUTAM Symposium on Asymptotics, Singularities and Homogenisation in Problems of Mechanics. Kluwer Academic Press, pp. 331–340.
Cherkaev, E., Zhang, D., 2003. Coupling of the effective properties of a random mixture through the reconstructed spectral representation. In: ETOPIM Proceedings, Physica B: Physics of Condensed Matter, vol. 338, pp. 16–23.
Cherkaev, E., Ou, M.-J., 2008. De-homogenization: reconstruction of moments of the spectral measure of composite. Inverse Problems 24, 065008.
Cowin, S.C., 1985. The relationship between the elasticity tensor and the fabric tensor. Mechanics of Materials 4, 137–147.
Cowin, S.C., 2001. Bone Mechanics Handbook. CRC Press.
Crolet, J.M., Aoubiza, B., Meunier, A., 1993. Compact bone: numerical simulation of mechanical characteristics. Journal of Biomechanics 26, 677–687.
Day, A.R., Thorpe, M.F., 1999. The spectral function of composite—the inverse problem. Journal of Physics: Condensed Matter 11, 2551–2568.
Day, A.R., Thorpe, M.F., Grant, A.R., Sievers, A.J., 2000. The spectral function of a composite from reflectance data. Physica B 279, 17–20.
Dell'Antonio, G.F., Figari, R., Orlandi, E., 1986. An approach through orthogonal projections to the study of inhomogeneous or random media with linear response. Annales de l'Institut Henri Poincaré 44 (1), 1–28.
Engstrom, C., 2006. Inverse bounds and bulk properties of complex-valued two-component composites. SIAM Journal on Applied Mathematics 67, 194–213.
Fang, M., Gilbert, R.P., Panchenko, A., Vasilic, A., 2007. Homogenizing the time-harmonic acoustics of bone: the monophasic case. Mathematical and Computer Modeling 46 (3-4), 331–340.
Gabriel, C., Gabriel, S., Corthout, E., 1996a. The dielectric properties of biological tissues: I. Literature survey. Physics in Medicine and Biology 41, 2231–2249.
Gabriel, S., Lau, R.W., Gabriel, C., 1996b. The dielectric properties of biological tissues: II. Measurements in the frequency range of 10 Hz to 20 GHz. Physics in Medicine and Biology 41, 2251–2269.
Gibson, L.J., 1985. The mechanical behavior of cancellous bone. Journal of Biomechanics 16, 317.
Gilbert, R.P., Liu, Y., Groby, J.P., Ogam, E., Wirgin, A., Xu, Y., 2009. Computing porosity of cancellous bone using ultrasonic waves, II: the muscle, cortical, cancellous bone system. Mathematical and Computer Modeling 50 (3–4), 421–429.
Golden, K., Papanicolaou, G., 1983. Bounds for the effective parameters of heterogeneous media by analytic continuation. Communications in Mathematical Physics 90, 473–491.
Goulet, R.W., Goldstein, S.A., Ciarelli, M.J., Kuhn, J.L., Brown, M.B., Feldkamp, L.A., 1994. The relationship between the structural and orthogonal compressive properties of trabecular bone. Journal of Biomechanics 27, 375–389.
Hellmich, C., Ulm, F.-J., Dormieux, L., 2004. Can the diverse elastic properties of trabecular and cortical bone be attributed to only a few tissue independent phase properties and their interaction? Biomechanics and Modeling in Mechanobiology 2 219–238.
Hodgskinson, R., Currey, J.D., 1990. The effect of variation in structure on the Young's modulus of cancellous bone: a comparison of human and non-human material. Proceedings of the Institution of Mechanical Engineers 204, 115–121.
Hollister, S.J., Fyhrie, D.P., Jepsen, K.J., Goldstein, S.A., 1991. Application of homogenization theory to the study of trabecular bone mechanics. Journal of Biomechanics 24, 825–839.
Hollister, S.J., Brennan, J.M., Kikuchi, N., 1994. A homogenization sampling procedure for calculating trabecular bone effective stiffness and tissue level stress. Journal of Biomechanics 27, 433–444.
Kabel, J., van Rietbergen, B., Odgaard, A., Huiskes, R., 1999a. Constitutive relationships of fabric, density, and elastic properties in cancellous bone architecture. Bone 25, 481–486.
Kabel, J., Odgaard, A., Van Rietbergen, B., Huiskies, R., 1999b. Connectivity and the elastic properties of cancellous bone. Bone 24, 115.
Kantor, Y., Bergman, D.J., 1982. Elastostatic resonances—a new approach to the calculation of the effective elastic constant of composites. Journal of the Mechanics and Physics of Solids 30, 335–376.
Kantor, Y., Bergman, D.J., 1984. Improved rigorous bounds on the effective elastic moduli of a composite material. Journal of the Mechanics and Physics of Solids 32, 41–62.
Keaveny, T.M., 1997. Mechanistic approaches to analysis of trabecular bone. Forma 12, 267.
Lakes, R.S., 2001. Viscoelastic properties of cortical bone. In: Cowin, S.C. (Ed.), Bone Mechanics Handbook second ed. CRC Press.
McPhedran, R.C., McKenzie, D.R., Milton, G.W., 1982. Extraction of structural information from measured transport properties of composites. Applied Physics A 29, 19–27.
McPhedran, R.C., Milton, G.W., 1990. Inverse transport problems for composite media. In: Geballe, T.H., et al. (Ed.), Physical Phenomena in Granular Materials, MRS Proceedings, vol. 195, pp. 257–274.
Milton, G.W., 1980. Bounds on the complex dielectric constant of a composite material. Applied Physics Letters 37, 300–302.
Milton, G.W., 2002. Theory of Composites. Cambridge Press.
Ou, M.J., Cherkaev, E., 2006. On the integral representation formula for a two-component elastic composite. Mathematical Methods in the Applied Sciences 29, 655–664.
Padilla, F., Laugier, P., 2005. Recent developments in trabecular bone characterization using ultrasound. Current Osteoporosis Reports 3 (2), 64–69.
Padilla, F., Grimal, Q., Laugier, P., 2008. Ultrasonic propagation through trabecular bone modeled as a random medium. Japanese Journal of Applied Physics 47 (5), 4220–4222.
Sanchez-Palencia, E., 1980. Non-homogeneous Media and Vibration Theory. Springer, Berlin.
Tokarzewski, S., Telega, J.J., Galka, A., 2001. Torsional rigidities of cancellous bone filled with marrow: the application of multipoint Pade approximants. Engineering Transactions 49, 135–153.
Tripp, A.C., Cherkaeva, E., Hulen, J., 1998. Bounds on the complex conductivity of geophysical mixtures. Geophysical Prospecting 46, 589–601.
Turner, C.H., Cowin, S.C., Rho, J.Y., Ashman, R.B., Rice, J.C., 1990. The fabric dependence of the orthotropic elastic constants of cancellous bone. Journal of Biomechanics 23, 549–561.
Van Rietbergen, B., Odgaard, A., Kabel, J., Huiskes, R., 1998. Relationships between bone morphology and bone elastic properties can be accurately quantified using high-resolution computer reconstructions. Journal of Orthopaedic Research 16, 23–28.
Van Rietbergen, B., Huiskies, R., 2001. Elastic constants of cancellous bone. In: Cowin, S.C. (Ed.), Bone Mechanics Handbook, second ed., CRC Press (Chapter 15).
Zoui, A., 2002. Continuum micromechanics: survey. Journal of Engineering Mechanics 128, 808–816.
Zhang, D., Cherkaev, E., 2008. Pade approximations for identification of air bubble volume from temperature or frequency dependent permittivity of a two-component mixture. Inverse Problems in Science and Engineering 16, 425–445.
Zhang, D., Cherkaev, E., 2009. Reconstruction of spectral function from effective permittivity of a composite material using rational function approximations. Journal of Computational Physics 228, 5390–5409.
Zysset, P.K., Goulet, R.W., Hollister, S.J., 1998. A global relationship between trabecular bone morphology and homogenized elastic properties. Journal of Biomechanical Engineering 120, 640–646.